Complex decay patterns in atomic core photoionization disentangled by ion-recoil measurements

Renaud Guillemin,[1,2,*] Cédric Bomme,[1,2] Thierry Marin,[1,2] Loic Journel,[1,2] Tatiana Marchenko,[1,2] Rajesh K. Kushawaha,[1,2] Nicolas Trcera,[3] Maria Novella Piancastelli,[1,2,†] and Marc Simon[1,2]

[1]*Université Pierre et Marie Curie, Université Paris 06, Laboratoire de Chimie Physique Matiere et Rayonement, 11 rue Pierre et Marie Curie, FR-75231 Paris Cedex 05, France*

[2]*Centre National de la Recherche Scientifique, Laboratoire de Chimie Physique Matiere et Rayonement (UMR7614), 11 rue Pierre et Marie Curie, FR-75231 Paris Cedex 05, France*

[3]*Synchrotron SOLEIL, l'Orme des Merisiers, Saint-Aubin, BP 48, FR-91192 Gif-sur-Yvette Cedex, France*

(Received 26 July 2011; published 29 December 2011)

Following core 1*s* ionization and resonant excitation of argon atoms, we measure the recoil energy of the ions due to momentum conservation during the emission of Auger electrons. We show that such ion momentum spectroscopy can be used to disentangle to some degree complex decay patterns, involving both radiative and nonradiative decays.

DOI: 10.1103/PhysRevA.84.063425 PACS number(s): 33.80.Eh, 34.50.Gb, 33.70.Ca

I. INTRODUCTION

The successful modeling of the interaction of x-ray radiation with a free atom is the gateway for extension of this approach to dynamical properties of material and bio systems. Complex phenomena such as decay dynamics following core excitation or core ionization in isolated many-electron atoms involve multistep vacancy cascades leading to multiply charged ions. Such processes are usually investigated by examining some of the possible channels one at a time and then trying to construct a consistent picture including the missing ones with the support of theoretical predictions. However, it would be highly desirable to devise a method by which a unified picture involving all possible channels at the same time is obtained by means of a single set of measurements. In this article, we present a tentative approach to such a method in a prototypical example, namely core-excited or core-ionized argon.

The decay processes following Ar 1*s* photoionization have been investigated with a variety of experimental and theoretical tools. The system relaxes the 1*s* vacancy through either photon emission (radiative decay) or electron emission (nonradiative decay). The relative weight of the radiative channel in Ar had been estimated to be between 8 and 14% [1,2]. In turn, the radiative and nonradiative pathways branch into several different subchannels. Radiative decay can lead to a state with one Ar 2*p* hole ($K\alpha$) or with a valence hole ($K\beta$). Nonradiative decay can proceed via a variety of vacancy creations in shallower levels, such as KLL (the 1*s* hole is filled and two vacancies are created in the Ar 2*p* and 2*s* levels), KMM (1*s* hole is filled and two valence vacancies are created), or a mixture such as KLM [3]. To further complicate the above picture, $K\alpha$ radiative decay leads to an intermediate state with still relatively deep holes and is likely to be followed by LMM Auger decay [1,3]; therefore the radiative and nonradiative channels are intertwined.

In particular, Auger $L_{2,3}MM$ decay patterns of K-excited or ionized Ar, following $K\alpha$ radiative decay, which are of special interest for the present experiments, have been investigated with electron spectroscopy [4,5], x-ray fluorescence, and Auger electron coincidence [6], photoion-Auger electron coincidence [7], and electron-ion and electron-electron coincidence techniques [3]. While the single-channel measurements underline the complexity of the Auger $L_{2,3}MM$ decay, coincidence experiments allow one to deepen the picture, connecting some selected Auger electron energies to a group of specific ions [7] or to $K\alpha$ emission followed by electron emission [6]. The relative weight of radiative versus nonradiative decay can be estimated from cross-section calculations but cannot be derived experimentally from the existing data sets.

In this article, we follow an approach that relies on the measurement for each ionic species of the recoil energy of the ion due to electron emission. Ion-recoil spectroscopy has recently gained attention in the gas phase, where it was efficiently used as a probe of two-photon ionization mechanisms on free-electron lasers [8], vibrational excitation [9], and interatomic Coulombic decay [10], and was demonstrated in solids and quantified similarly to the Mössbauer effect [11]. We report here the use of ion-recoil momentum spectroscopy to disentangle multiple decay patterns. For momentum conservation, the departing electron induces recoil on the ion which is directly proportional to the ion mass and to the electron velocity. From the ion-recoil momentum vector, it is possible to correlate the creation of a specific charged species Ar^{n+}, with $n = 1$–7, to a radiative, nonradiative, or mixed multistep process following Ar 1*s* photoionization or resonant excitation. It is possible to distinguish between an ion produced by the emission of very fast electrons (2600–2900-eV kinetic energy), which implies KLL or KLM Auger electron emission, therefore Auger decay as the first step, or electrons with lower energy (200-eV kinetic energy), which implies LVV Auger decay, and therefore $K\alpha$ radiative decay as the first step followed by Auger. By evaluating the relative abundance of the various ions from the mass spectrum, and knowing by which pathway each ion is produced, we can estimate the relative percentage of radiative versus nonradiative decay.

*renaud.guillemin@upmc.fr

†Permanent address: Department of Physics and Astronomy, Uppsala University, PO Box 516, SE-751 20 Uppsala, Sweden.

 ©2011 American Physical Society

II. EXPERIMENTAL SETUP

We performed the measurements on beamline LUCIA [12] at SOLEIL, Orsay-France. The beamline delivers a linearly polarized monochromatic photon beam in the 0.8- to 8-keV energy range. The photon energy was calibrated on the argon $1s \rightarrow 4p$ resonance at 3203.54 eV and ionization potential (IP or $V_{\rm ion}$) at 3206.26 eV [13]. The data were obtained using a newly developed setup, CELIMENE, that belongs to the extended family of cold target recoil momentum spectroscopy (COLTRIMS) apparatuses [14,15]. The instrument, which will be described in detail in a future publication, is based on the double-velocity spectrometer developed in the group of D. Dowek in Orsay, France [16]. In this study, the photon beam crossed a cold supersonic jet of argon at a right angle, forming an interaction volume of approximately $0.1 \times 1 \times 2$ mm^3. Electrons and ions were separated and accelerated toward facing time-of-flight (TOF) spectrometers perpendicularly to the photon beam and atomic jet, with a static electric field (typically 20 V/cm) chosen to collect within a 4π solid angle all the photoelectrons and ions with a maximum kinetic energy of 8 eV in this study. The particles were detected with 80-mm position sensitive detectors using delay lines [17]. Both time of flight and impact positions of the ions and electrons detected in coincidence were recorded, allowing us thus to determine the full momentum vector of all particles for each ionization event [14]. The electron and ion spectrometers are strictly identical, and calibration was made using the photoelectron emission from Ar^+ measured 6 eV above the threshold, which decays only through radiative emission; no Auger electron is emitted, and no postcollision interaction (PCI) occurs. Because the ion velocities are deduced from impact positions and time of flight, the resulting momentum resolution achieved is not constant across the range of measurements and is higher for slow ions. With 10 V/cm of extraction field, the momentum resolution was found to be 3 a.u. at 3.5 a.u. and 6.5 a.u. at 12 a.u. This limited momentum resolution is essentially due to the finite, and rather large, size of the interaction volume. Improvement in the design and operation of the supersonic jet should increase dramatically the resolution.

In this configuration, the setup was used to measure the (V_x, V_y, V_z) components, with (x, y) in the plane of the detector, of the velocity vectors $\mathbf{V}_{n^+}$ and $\mathbf{V}_{e^-}$ of each (Ar^{n+}, e^-) coincident event, where e^- is the photoelectron above the ionization threshold, or a slow shakeoff electron for measurements done at the $1s \rightarrow 4p$ resonance. The coincident detection of an energy-analyzed electron allows us to filter out contributions from shells other than the K shell.

III. RESULTS

A. Ion branching ratios

The branching ratios of the various decay channels are deduced in part from the branching ratios of the different ionic channels. However, the probability of electron recapture affects these ratios at photon energies close to IP [18]. We measured the ion branching ratios at 6, 4, and 2 eV above the threshold. We used as a reference the TOF spectrum measured at $h\nu = 3212.3$ eV, 6 eV above the threshold, where it was shown that no electron recapture occurs from ion yield measurements [13]. The probability of recapture for each ion as a function of $E_{\rm exc} = h\nu - V_{\rm ion}$ is given by

$$N_q(E_{\rm exc}) = N_{q+1\rightarrow q}(E_{\rm exc}) + N_q(6) - N_{q\rightarrow q-1}(E_{\rm exc}), \quad (1)$$

with $N_{7+1\rightarrow 7} = 0$ and $N_{1\rightarrow 1-1} = 0$. Calculated values for recapture probability as a function of photon energy and ionic charge above the threshold are given in Table I. Finally, we obtain for the various Ar^{n+} ion charges following the branching ratios (±0.15%): Ar^+ (0.9%), Ar^{2+} (9.7%), Ar^{3+} (13.7%), Ar^{4+} (46.3%), Ar^{5+} (23.5%), Ar^{6+} (5.5%), and Ar^{7+} (0.5%), found in good agreement with the values reported in the literature [1,13]. Total electron recapture was found to amount to 17.9% at 2 eV above the threshold, and 7.5% at 4 eV. Along the $1s \rightarrow 4p$ resonance, the branching ratios measured are (±0.15%): Ar^+ (3.1%), Ar^{2+} (7.5%), Ar^{3+} (25.6%), Ar^{4+} (39.6%), Ar^{5+} (19.7%), Ar^{6+} (4.2%), and Ar^{7+} (0.4%).

TABLE I. Probability of electron recapture as a function of photon energy above threshold and ionic charge. Numbers in italics refer to the number of ions coming from the recapture of an electron by the ion species of charge $q + 1$. Zeros in bold face are assumed.

	Branching ratios (%)						
$h\nu$ (eV)	Ar^+	Ar^{2+}	Ar^{3+}	Ar^{4+}	Ar^{5+}	Ar^{6+}	Ar^{7+}
3203.54 ($1s \rightarrow 4p$)	3.1	7.5	25.6	36.6	19.7	4.2	0.4
3208.3 ($V_{\rm ion} + 2$ eV)	1.4	13.5	16.3	44.1	19.9	4.4	0.4
from recapture	*0.5*	*4.3*	*7.0*	*4.8*	*1.2*	*0.1*	*0*
3210.3 ($V_{\rm ion} + 4$ eV)	1.1	11.3	14.2	46.1	22.0	4.8	0.4
from recapture	*0.3*	*1.9*	*2.4*	*2.2*	*0.7*	*0.1*	*0*
3212.3 ($V_{\rm ion} + 6$ eV)	0.86	9.7	13.6	46.3	23.5	5.46	0.5
from recapture	***0***	***0***	***0***	***0***	***0***	***0***	***0***

B. Ion-recoil energy

The energy spectra derived from the velocity vectors for each Ar^{n+} ion ($n = 2$–4) are shown in Fig. 1(a) as two-dimensional maps that represent for each ionization event the photoelectron energy as a function of ion energy, from measurements done at 3208.3 eV photon energy, 2 eV above the threshold, with a 10-V/cm extraction field. These maps contain a wealth of information on the ionization process (PCI, decay pathways, etc.). In the following, we will only focus on the energy of the ions. It is clear from the maps in Fig. 1(a) that the three ions shown here possess different energy distributions. Ar^{2+} has a very small kinetic energy, and most events are below 10 meV. Ar^{3+} has a more extended energy distribution that includes a low-energy component comparable to Ar^{2+} [labeled (1) in Fig. 1(a)] and a larger component with a maximum at around 35 meV [labeled (2) in Fig. 1(a)]. Ar^{4+} shows only a high-energy component centered around 35 meV.

C. Auger electron momentum

In molecular photoionization, the momentum of the fragment ions mainly comes from kinetic-energy release during the dissociation of the molecule (see for instance [19,20]). For an isolated atom, the momentum gained by the ion during photoionization is mainly due to momentum conservation

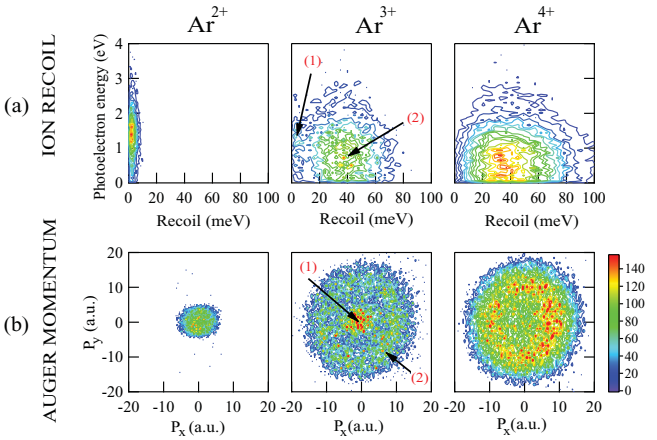

FIG. 1. (Color online) (a) Kinetic-energy correlation diagram: photoelectron energy as a function of ion-recoil energy, measured at 3208.3-eV photon energy, 2 eV above threshold. (b) Auger electron momentum derived from the ion-recoil by momentum conservation.

when the atom emits an electron. The ion energy measured in Fig. 1(a) is thus a recoil energy. The momentum of a 2-eV photoelectron (0.38 a.u.) is small compared to the momentum transfer due to the emission of a 200-eV Auger electron (similar to a LMM Auger electron in Ar), which corresponds to 3.8 a.u., or a 2700-eV Auger electron (similar to a KLL Auger electron in Ar), which corresponds to 14 a.u. Therefore the ion momentum distribution reflects the electronic decay that follows core excitation. This property was used recently by A. L. Landers *et al.* [21] to study the angular correlation between photoelectrons and Auger electrons after K-shell ionization in neon, at 873 eV. In this case, recoil momentum analysis was limited to Ne^{2+} "kicked" by an 800-eV Auger electron (7.7 a.u.). In the case of argon K-shell ionization, the many decay pathways lead to the formation of highly charged ions and the emission of Auger electrons with very different momenta, providing the opportunity to test our primary assumption that relaxation pathways, associated with undetected particles (x-ray photons or Auger electrons), can be determined via ion momentum spectroscopy.

The three components (P_x, P_y, P_z) of the momentum vector $\mathbf{P}_\mathrm{A}$ associated with Auger emission were determined from the measurement of the ion velocity vectors $\mathbf{V}_{n^+}$, by momentum conservation: $\mathbf{P}_{\mathrm{A}n^+} = -m_\mathrm{Ar}\mathbf{V}_{n^+}$. Because the interaction region between the supersonic jet and the photon beam has a finite size, it must be taken into account. All momenta were normalized using Ar^+ above IP, which can only be formed above the threshold by $K\beta$ radiative decay and therefore does not have any measurable momentum. A $K\beta$ photon ($h\nu = 3190$ eV) carries a momentum of 0.8 a.u., which when transferred to the ion leads to a kinetic energy of 0.15 meV, well below the measurable level. It is thus neglected. On the same magnitude, the momentum transfer due to the slow photoelectron could be taken into account because its kinetic energy was directly measured. The Auger electron momentum component P_y is shown in Fig. 1(b) as a function of P_x for each Ar^{n+} ion ($n = 2$–4) (the third component P_z is not shown). The data for the ion species with higher charge are similar

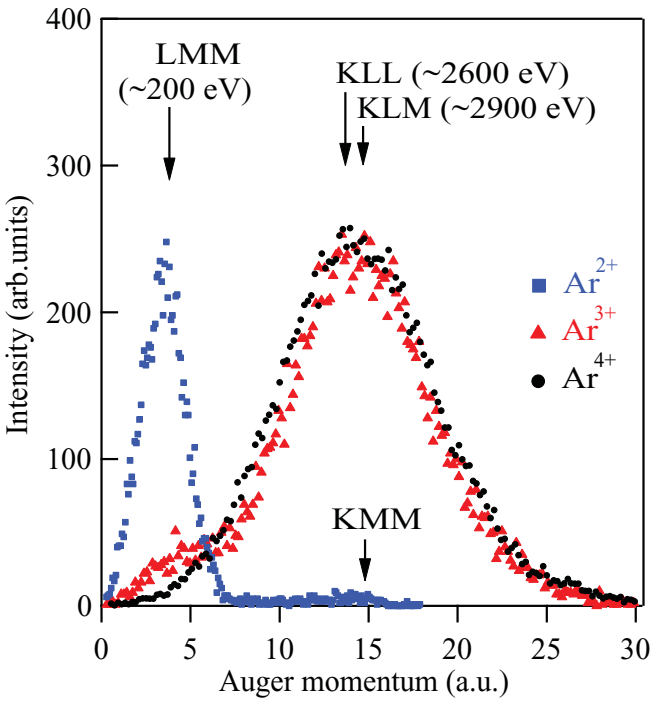

FIG. 2. (Color online) Norm of the Auger electron momentum vector for Ar^{2+}, Ar^{3+}, and Ar^{4+} in a histogram. The intensity of the spectra is arbitrarily normalized. The data were collected at 3208.3 eV, 2 eV above the K threshold [13].

to Ar^{4+}. In the case of cascade Auger emission, $\mathbf{P}_\mathrm{A}$ includes all the contributions from subsequent Auger electrons emitted isotropically and not only the momentum of a single Auger electron. However, we can assume the momentum distribution mainly represents the first Auger electron, which carries the largest kinetic energy. Following a stepwise process, in which electrons are not angularly correlated, the second step decay only widens the momentum distribution. The momenta in Fig. 1(b) show the same differences seen in the ion-recoil energy. Notably, Ar^{3+} shows two momentum components as two concentric rings labeled (1) and (2). The magnitude of the full momentum vector $\mathbf{P}_\mathrm{A}$ was derived from the three components (P_x, P_y, P_z) by integration over all emission angles. The resulting Auger momentum spectra are shown as histograms in Fig. 2 (2 eV above IP) and in Fig. 3 (on resonance) for each Ar^{n+} ion ($n = 2$–4).

IV. DISCUSSION

These momentum spectra draw a clear picture of the decay process. For some of the ions, the yield is correlated to only one electron momentum. Ar^{2+} above IP, in Fig. 2, and Ar^+ on resonance, in Fig. 3, are associated with the emission of only one electron momentum around 3.8 a.u. (the 200-eV kinetic-energy range). It implies that the main decay channel to produce them is $K\alpha$ x-ray emission followed by Auger LVV electron emission [1,3]. On the other hand, Ar^{4+} above IP, Fig. 2, and Ar^{3+} on resonance, Fig. 3, are associated with fast electrons with a momentum around 14 a.u. (the 2600–2900-eV kinetic-energy range). They originate from a primary Auger decay (KLL or KLM) [7,22], followed by an Auger cascade.

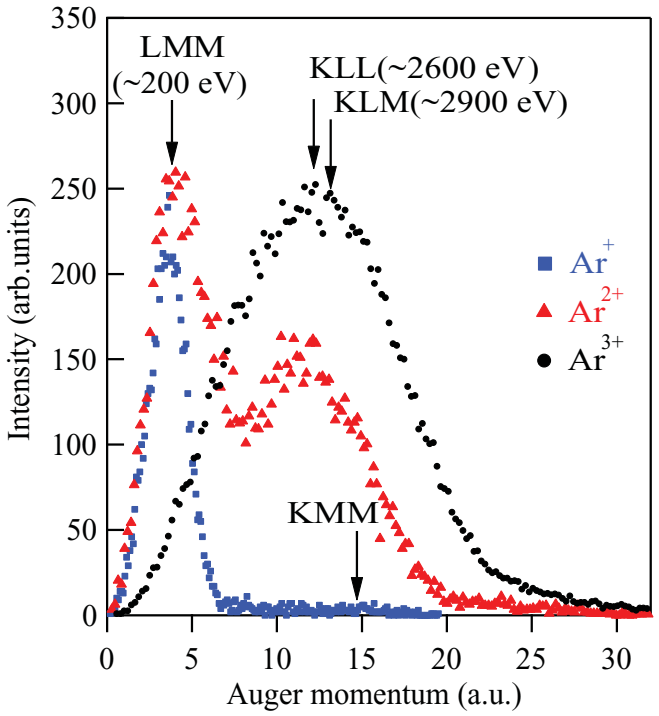

FIG. 3. (Color online) Norm of the Auger electron momentum vector for Ar^{2+}, Ar^{3+}, and Ar^{4+}. The intensity of the spectra is arbitrarily normalized. The data were collected at the $1s \rightarrow 4p$ resonance, 3203.54 eV [13].

The higher charge ions Ar^{5+} and Ar^{6+} (not shown for clarity) produced by cascade processes show the same behavior. Ar^{3+} above IP and Ar^{2+} on resonance are correlated to contributions from both low and high electron momenta, respectively 3.8 and 14 a.u., which correspond to feature (1) and (2) in Fig. 1. Although KMM processes are rather unlikely, we observe a weak peak for Ar^{2+} above IP at high momentum, which corresponds to KMM transitions at Auger kinetic energies around 3000 eV. KMM emission represents 4.1% of the partial Ar^{2+} yield, which itself represents 9.7% of the total ion yield at 6 eV above the threshold. We observed the same contribution to the Ar^{2+} yield at 4 and 6 eV above IP, which rules out electron recapture from Ar^{3+}. From this we can derive that KMM decay represents $0.4 \pm 0.3\%$ of the total decay (radiative and nonradiative). A small contribution from KMM decay, $<0.1\%$, is observed in the momentum spectrum associated with Ar^{+} at resonance. Above IP, the amount of $K\beta$ emission can be taken as equal to the amount of Ar^{+} produced, as no other process can lead to the singly charged ion in the absence of electron recapture. After resonant excitation followed by $K\beta$ emission, neutral argon is produced and the amount of $K\beta$ decay cannot be measured with the present method. The amount of $K\alpha$ emission can be derived from the emission intensity in LMM decay from Ar^{2+} and Ar^{3+} in Fig. 2 and from Ar^{+} and Ar^{2+} in Fig. 3. Intensities for the various decay channels derived from our measurements are found in good agreement with the theoretical intensities reported in [1] and are summarized in Table II.

The general framework of our interpretation is confirmed by the patterns above and below IP, which are the same if the ion charges are shifted by one, apart from some differences in the intensity of the respective contributions. Special cases are Ar^{3+} above IP (Fig. 2) and Ar^{2+} on resonance (Fig. 3). These species are produced by emission of either fast or slow electrons, with a different intensity ratio between the two channels above and below IP. We interpret this behavior as related to two main pathways, radiative decay followed by Auger electron emission accompanied by shakeoff processes, for the slow electron emission, and Auger KLM for the fast electron emission. The total percentage of shakeoff processes is estimated as $\pm 2\%$ [7]. The difference in the branching between radiative and nonradiative decay for Ar^{3+} above the threshold and Ar^{2+} on resonance, mainly the higher rate of radiative decay followed by LMM observed on resonance, can be attributed to the fact that on resonance the electron loosely bound and likely to be "shaken off" is the excited electron in the $4p$ level, present on resonance but not above the threshold. While it is known from literature that the percentage of radiative decay for an Ar $1s$ core hole is around 11% [1], it is difficult to measure by other methods and usually requires a combination of techniques. Here a direct assessment of $10.6 \pm 0.2\%$ above IP can be given. This result confirms the sensitivity of ion-recoil measurements to the study of decay channels as a whole.

TABLE II. Experimental (this study) and theoretical [1] branching ratios presented as percentages, for the various decay pathways in K-shell resonantly excited or ionized argon atoms.

Transition	Experiment ($1s \rightarrow 4p$)	Experiment ($1s \rightarrow$ continuum)	Theory [1] ($1s \rightarrow$ continuum)
$K\beta$	—	0.9 ± 0.15	0.77
$K\alpha$	8.0 ± 0.15	9.8 ± 0.15	10.92
KMM	$<0.1 \pm 0.3$	0.4 ± 0.3	0.43
$KLM + KLL$	92 ± 0.15	88.9 ± 0.15	87.89

V. CONCLUSION

In conclusion, we have shown on a simple atomic system that ion-recoil momentum spectroscopy can be used to probe intricate decay processes that follow core ionization or excitation. The method is also unique in providing direct information on the branching between radiative and nonradiative decay. We believe this method can be generalized to the study of more complex systems and can be a powerful tool to investigate, for instance, ultrafast dissociation processes in molecular photofragmentation [23], to study the competition between radiative and nonradiative decay as a function of chemical environment in molecular photoionization, multiphoton processes on free-electron lasers sources [8], and in solids where recoil effects can be important in the fast developing field of high-energy photoelectron spectroscopy [11].

ACKNOWLEDGMENTS

M. N. P., Ta. M., and R. K. K acknowledge the financial support of Agence Nationale de la Recherche through Grant No. CHEX2010. The authors thank SOLEIL for providing the facility and support (Project No. 20090604).

[1] A. G. Kochur, V. L. Sukhorukov, A. I. Dudenko, and Ph. V. Demekhin, J. Phys. B **28**, 387 (1995).
[2] A. Kahoul, A. Abassi, B. Deghfel, and M. Nekkab, Rad. Phys. Chem. **80**, 369 (2011), and references therein.
[3] U. Alkemper, J. Doppelfeld, and F. von Busch, Phys. Rev. A **56**, 2741 (1997), and references therein.
[4] J. W. Cooper, S. H. Southworth, M. A. MacDonald, and T. LeBrun, Phys. Rev. A **50**, 405 (1994).
[5] F. von Busch, J. Dopplefeld, C. Gunther, and E. Hartmann, J. Phys. B: At. Mol. Opt. Phys. **27**, 2151 (1994).
[6] U. Arp, T. LeBrun, S. H. Southworth, M. A. MacDonald, and M. Jung, Phys. Rev. A **55**, 4273 (1997).
[7] J. C. Levin, C. Biedermann, N. Keller, L. Liljeby, C. S. O, R. T. Short, I. A. Sellin, and D. W. Lindle, Phys. Rev. Lett. **65**, 988 (1990).
[8] A. Rudenko *et al.*, Phys. Rev. Lett. **101**, 073003 (2008).
[9] T. D. Thomas *et al.*, J. Chem. Phys. **128**, 144311 (2008).
[10] K. Kreidi *et al.*, Phys. Rev. Lett. **103**, 033001 (2009).
[11] Y. Takata *et al.*, Phys. Rev. B **75**, 233404 (2007).
[12] A.-M. Flank *et al.*, Nucl. Instrum. Methods Phys. Res. B **246**, 269 (2006).
[13] K. Ueda, E. Shigemasa, Y. Sato, A. Yagishita, M. Ukai, H. Maezawa, T. Hayaishi, and T. Sasaki, J. Phys. B: At. Mol. Opt. Phys. **24**, 605 (1991).
[14] R. Dörner, V. Mergel, O. Jagutzki, L. Spielberger, J. Ullrich, R. Moshammer, and H. Schmidt-Böcking, Phys. Rep. **330**, 95 (2000).
[15] J. Ullrich, R. Moshammer, A. Dorn, R. Dörner, L. Ph. H. Schmidt, and H. Schmidt-Böcking, Rep. prog. Phys. **66**, 1463 (2003).
[16] M. Lebech, J. C. Houver, and D. Dowek, Rev. Sci. Instrum. **73**, 1866 (2002).
[17] O. Jagutzki, V. Mergel, K. Ullmann-Pfleger, L. Spielberger, U. Spillmann, R. Dörner, H. Schmidt-Böcking, Nucl. Instrum. Methods Phys. Res. A **477**, 244 (2002).
[18] T. Hayaishi, E. Murakami, E. Shigemasa, A. Yagishita, F. Koike, and Y. Morioka, J. Phys. B: At. Mol. Opt. Phys. **28**, 5261 (1995).
[19] A. Lafosse, M. Lebech, J. C. Brenot, P. M. Guyon, O. Jagutzki, L. Spielberger, M. Vervloet, J. C. Houver, and D. Dowek, Phys. Rev. Lett. **84**, 5987 (2000).
[20] L. Journel *et al.*, Phys. Rev. A **77**, 042710 (2008).
[21] A. L. Landers *et al.*, Phys. Rev. Lett. **102**, 223001 (2009).
[22] G. B. Armen, J. C. Levin, and I. A. Sellin, Phys. Rev. A **53**, 772 (1996).
[23] D. L. Hansen *et al.*, Phys. Rev. A **57**, 2608 (1998).